Original Article

Association between descending aorta wall thickness or wall area and cardiovascular disease risk factors in cardiovascular disease-free patients: a study based on water-calcium material decomposition and subtraction-based computed tomography dark-blood imaging

Yan Qi[1], Ye Huang[2], Haichao Liu[1], Yiming Yang[1], Yan Jiang[1], Zhiyuan Chen[1], Long Li[1], Mengya Guo[3], Jianying Li[3], Dongjing Zhou[1], Yupin Liu[1]

[1]Department of Radiology, The Second Affiliated Hospital of Guangzhou University of Chinese Medicine, Guangzhou, China; [2]Second Clinical Medical College of Guangzhou University of Traditional Chinese Medicine, Guangzhou, China; [3]CT Imaging Research Center, GE HealthCare, Guangzhou, China

Contributions: (I) Conception and design: Y Qi, Y Liu, D Zhou; (II) Administrative support: Y Liu; (III) Provision of study materials or patients: L Li, Z Chen, Y Yang; (IV) Collection and assembly of data: Y Qi, Y Huang, H Liu, Y Jiang; (V) Data analysis and interpretation: Y Qi, M Guo, J Li; (VI) Manuscript writing: All authors; (VII) Final approval of manuscript: All authors.

Correspondence to: Yupin Liu, PhD; Dongjing Zhou, MD. Department of Radiology, The Second Affiliated Hospital of Guangzhou University of Chinese Medicine, 111 Dade Road, Guangzhou 510120, China. Email: mdliuyupin@163.com; 56950762@qq.com.

Background: Due to the low contrast between the vascular lumen and vessel wall, conventional computed tomography (CT) is not an effective method for visualizing the vessel wall. The purpose of this study was to assess the feasibility of vessel wall visualization using contrast-enhanced dual-energy CT (DECT)-derived water-calcium material decomposition (WMD) and subtraction-based dark-blood imaging (DBI). An additional objective of this study was to determine the association of descending aorta wall thickness (WT) and wall area (WA) with cardiovascular disease (CVD) risk factors and to ascertain the potential of DECT-derived WT and WA as image markers for identifying individuals at high risk for future CVD.

Methods: In this cross-sectional study, virtual noncontrast (VNC), subtraction-based DBI, and WMD images of 106 patients were generated from the arterial-phase DECT data files. To assess the vessel wall visualization, the contrast-to-noise ratios (CNRs) of the descending aorta between the vessel wall and lumen or periaortic fat ($CNRs_{wall\text{-}lumen}$ *or* $CNRs_{wall\text{-}fat}$) were calculated and compared in VNC, subtraction-based DBI, and WMD images. Subsequently, two radiologists independently assessed the vessel wall visualization of these three kinds of images using a four-point scale. To evaluate the association between WT or WA and CVD risk factors, descending aortic WT and WA were measured in the subtraction-based DBI and WMD images, while interobserver agreement was assessed through intraclass correlation coefficients (ICCs). The relationship between the WT or WA and CVD risk factors was determined using univariate and multiple regression analyses.

Results: Both WMD and subtraction-based DBI images demonstrated superior $CNRs_{wall\text{-}lumen}$ and qualitative scores as compared to VNC images ($CNRs_{wall\text{-}lumen}$: 0.59±0.47, 4.36±2.14, and 4.81±3.28, respectively; qualitative scores: 1.04±0.71, 2.53±0.50, and 2.92±0.27, respectively; for virtual non-contrast, subtraction-based DBI and WMD images respectively, all P values <0.05), which indicated better image qualities for vessel wall imaging. The mean descending aorta WT values were 2.18±0.27 and 2.17±0.27 mm for observer 1 and 2.14±0.27 and 2.15±0.26 mm for observer 2 in the subtraction-based DBI and WMD images, respectively. Age and smoking status were predictors for both WT and WA, while males had higher

© AME Publishing Company.

WA values than did females. Blood pressure was only significant for WA measured in subtraction-based DBI.

Conclusions: Both subtraction-based DBI and WMD images in DECT can be used to effectively visualize vessel walls and measure WT and WA, with both measurements demonstrating a positive correlation with CVD risk factors of age and smoking.

Keywords: Water-calcium material decomposition (WMD); subtraction-based dark-blood imaging (DBI); wall thickness (WT); wall area (WA)

Submitted Jul 05, 2024. Accepted for publication Oct 30, 2024. Published online Dec 30, 2024.
doi: 10.21037/qims-24-1371
View this article at: https://dx.doi.org/10.21037/qims-24-1371

Introduction

Cardiovascular disease (CVD) is the primary cause of global morbidity and mortality, resulting in approximately 19.8 million deaths in 2022 (1). Interventions and treatments in the early stages of CVD hold the potential to reduce the incidence of adverse cardiovascular events. However, the early stages of CVD manifest as vessel wall thickening and plaque formation in vessel wall images, with no overt clinical symptoms. Studies have indicated that the wall thickness (WT) of large arteries correlates with the burden of atherosclerosis and serves as a predictive marker for cardiovascular events (2,3).

Several noninvasive vessel wall-imaging techniques are available for WT evaluation, including ultrasound (US) (4), magnetic resonance imaging (MRI) (5), and computed tomography (CT) (6,7). Prior studies have focused on using US to assess vessel WT in the extracranial carotid arteries and detecting aneurysms in the aortic root. However, US image quality can be affected by patient size and the competency of the operator. Magnetic resonance (MR) is the preferred noninvasive modality for vessel wall assessment and diagnosis (8,9). High-resolution black-blood MRI enables the evaluation of thoracic aortic wall area (WA) and plaque characteristics, which act as independent predictive factors for CVD (10). However, MRI scanning is often time-consuming and contraindicated in patients with metal implants or claustrophobia. CT plays a crucial role in diagnosing vessel stenosis. Aorta diameters measured in CT images correlate with CVD risk factors, as demonstrated in the Framingham Heart Study offspring cohort (n=3,431) (11). However, vessel wall evaluation based on CT remains challenging due to the low contrast between the vessel wall and the peripheral structures, which is particularly evident in contrast-enhanced CT images.

Recently, several commercial vendors have introduced dark-blood CT methods for vessel wall imaging. Canon's dark-blood CT images, based on the subtraction between registered delayed and arterial phase images, have been investigated in the context of carotid artery (12) and Takayasu arteritis (13). The clinical potential of Philips' dark-blood CT images has been demonstrated in terms of aortic intramural hematoma (14) and vascular involvement in pancreatic cancer (15). Furthermore, GE HealthCare's subtraction-based dark-blood imaging (DBI) is a technique based on contrast-enhanced dual-energy CT (DECT) images, generated by subtracting the virtual noncontrast (VNC) image from a 70-keV virtual monochromatic image (VMI) with suitable weights. However, the related investigations on GE HealthCare's subtraction-based DBI are scarce. Interestingly, in our clinical practice, the water-calcium material decomposition (WMD) images in DECT have also exhibited excellent capability in vessel wall visualization.

The measurement of arterial WT in various vascular territories is of considerable interest, as it has the potential to correlate with cardiovascular risk and predict future cardiovascular events. Numerous investigations have examined the relationship between vessel WT and CVD risk factors using MR vessel wall imaging to explore its potential in diagnosing early-stage CVD (6,10,16); however, previous CT imaging studies have primarily focused on vessel diameter (11,17,18). Therefore, in this study, we first aimed to assess the feasibility of vessel wall visualization based on GE HealthCare's subtraction-based DBI and WMD images. Subsequently, we evaluated the association of DECT-derived WT and WA with CVD risk factors to clarify the potential of DECT-derived WT and WA as image markers for identifying high-risk individuals for CVD within a CVD-free population. We present this article in accordance with the STROBE reporting checklist (available

© AME Publishing Company.

at https://qims.amegroups.com/article/view/10.21037/qims-24-1371/rc).

Methods

Study population

This single-center retrospective study was conducted in accordance with the Declaration of Helsinki (as revised in 2013) and was approved by the Ethics Committee of Guangdong Provincial Hospital of Chinese Medicine (No. ZE2023-422-01). The requirement for individual consent was waived due to the retrospective nature of the analysis. From February to October 2023, a total of 106 clinical CVD-free patients admitted to Guangdong Provincial Hospital of Chinese Medicine were enrolled. These patients underwent arterial-phase DECT acquisition of the chest/chest-abdomen for clinical diagnosis. Patients (I) with severe atherosclerosis including mural thrombus, aortic dissection aneurysm, and intra-aortic hematoma or (II) those with a stent were excluded.

Image acquisition and reconstruction

All examinations were performed on a DECT scanner (Revolution Apex; GE HealthCare, Chicago, IL, USA) using the gemstone spectral imaging (GSI) mode under the following scanning parameters: rapid kilovolt (kV) switching between 80 and 140 kVp; tube current, 405 mA; helical pitch, 0.992:1; rotation time, 0.8 seconds; reconstruction method, 50% adaptive statistical iterative reconstruction V (ASIR-V) with standard reconstruction kernel; display field-of-view (DFOV), 50 cm; and reconstruction matrix, 512×512. For contrast enhancement, an iodinated contrast agent (370 mgI/mL Optiray, 1 mL/kg body weight; Bayer, Leverkusen, Germany) was injected into an antecubital vein at an injection rate of 4 mL/s and was followed by a saline flush at the same rate. CT acquisitions of the arterial phase were initiated 6 seconds after a trigger threshold of 150 Hounsfield units (HU) (Smart Prep, GE HealthCare) was reached in the tracheal bifurcation level of the descending aorta; moreover, those in portal venous phases were initiated 20–25 seconds after the end of the arterial phase.

Upon completion of the scanning, the VNC image was reconstructed simultaneously and transferred to the Advantage Workstation (AW) 4.7 (GE HealthCare). In the GSI Volume Viewer in AW 4.7, the WMD and 70-keV VMI acquired during the arterial phase were obtained using the DECT datafiles. Subtraction-based DBI was generated by subtracting the VNC image from the 70-keV VMI (*Figure 1*) according to the following formula:

$$Subtraction\text{-}based\ DBI = p \times VNC - (1-p) \times VMI_{70\ keV} \quad [1]$$

where the parameter p represents the weight of the subtraction between these two image sets. In accordance with practical findings, the vessel wall display was optimal in the subtraction-based DBI when p ranged from 0.7 to 0.8.

Image quality assessment and WT and WA measurement

In the quantitative analysis, the descending aorta at the diaphragm level was selected for WT and WA measurements. On the magnified axial WMD image (DFOV 10.6 cm × 7.6 cm), the wall of the descending aorta was partitioned into four equiangular quadrants, and four small regions of interest (ROIs) were manually placed within these quadrants to cover as much of the WA as possible, with any heterogeneity in the wall being avoided. On the same image slice, the lumen and periaortic ROIs were manually placed in the corresponding region. Furthermore, these ROIs were automatically copied and placed onto the VNC and subtraction-based DBI in the exactly the same position. The mean and standard deviation of the HU values in each ROI were then recorded. To quantify the feasibility of WMD and subtraction-based DBI for vascular wall imaging, the contrast-to-noise ratios (CNRs) of the descending aorta between the vessel wall and lumen or periaortic fat ($CNRs_{wall\text{-}lumen/fat}$) were calculated using the following formula and compared:

$$CNR_{wall\text{-}lumen/fat} = \frac{\left| mean\ HU_{wall} - mean\ HU_{lumen/periaortic\ fat} \right|}{\sqrt{\frac{1}{2}\left(SD\ HU_{wall}^2 + SD\ HU_{lumen/periaortic\ fat}^2 \right)}} \quad [2]$$

where $mean\ HU_{wall}$ and $SD\ HU_{wall}$ and $mean\ HU_{lumen/periaortic\ fat}$ and represent the average and standard deviation of HU values in the ROIs of the wall and lumen/periaortic fat, respectively. All measurements related to CNR were performed by a radiologist with 13 years of experience in radiology. In the evaluation of the qualitative image quality of vessel wall imaging across these three types of images, two radiologists (observers 1 and 2 with 13 and 7 years of experience in radiology, respectively) independently reviewed and evaluated the image quality. The following four-point Likert scale, based on the conspicuity of the inner and outer vessel wall and the smoothness of inner

© AME Publishing Company.

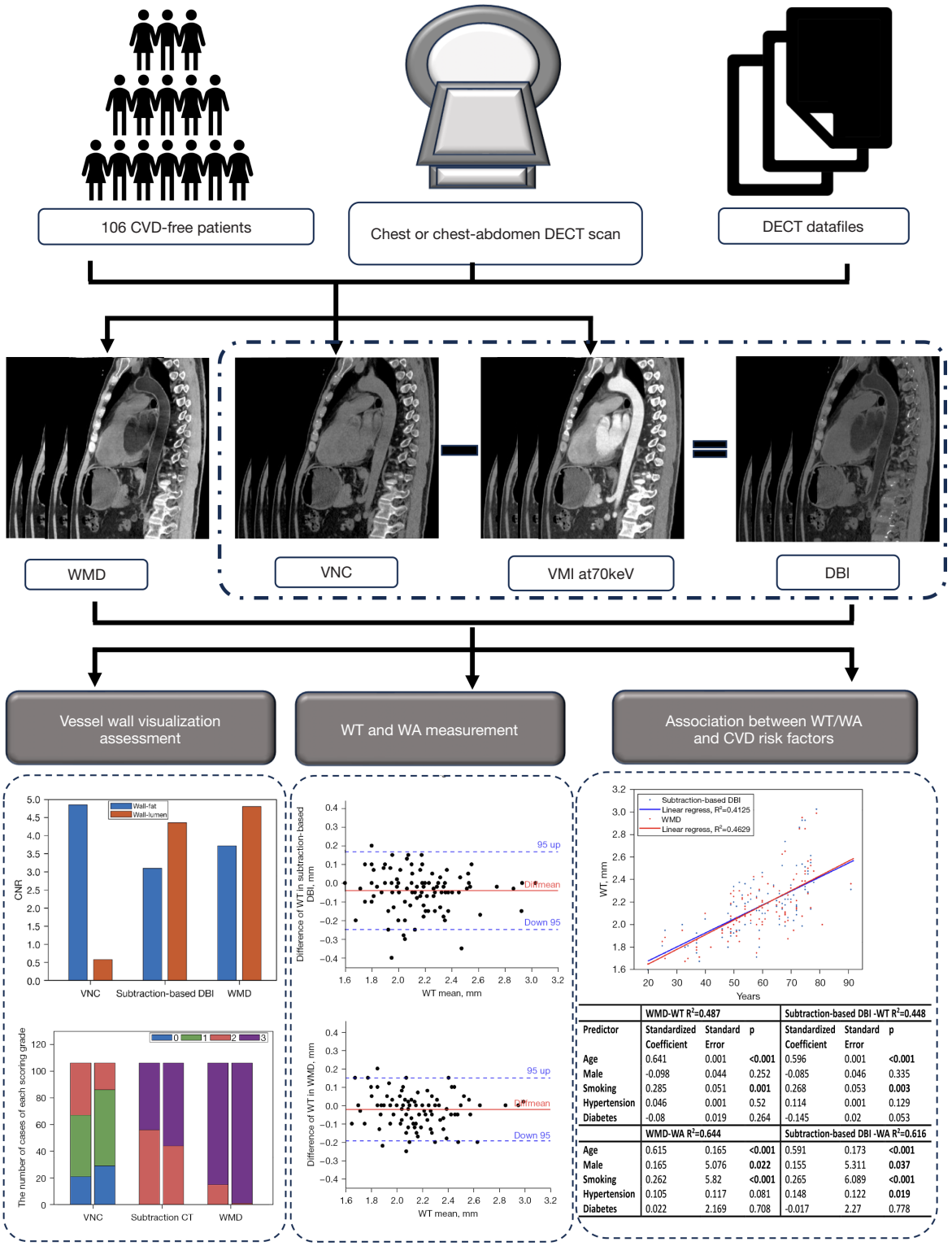

	WMD-WT R^2=0.487			Subtraction-based DBI -WT R^2=0.448		
Predictor	Standardized Coefficient	Standard Error	p	Standardized Coefficient	Standard Error	p
Age	0.641	0.001	<0.001	0.596	0.001	<0.001
Male	-0.098	0.044	0.252	-0.085	0.046	0.335
Smoking	0.285	0.051	**0.001**	0.268	0.053	**0.003**
Hypertension	0.046	0.001	0.52	0.114	0.001	0.129
Diabetes	-0.08	0.019	0.264	-0.145	0.02	0.053
	WMD-WA R^2=0.644			Subtraction-based DBI -WA R^2=0.616		
Age	0.615	0.165	<0.001	0.591	0.173	<0.001
Male	0.165	5.076	**0.022**	0.155	5.311	**0.037**
Smoking	0.262	5.82	<0.001	0.265	6.089	<0.001
Hypertension	0.105	0.117	0.081	0.148	0.122	**0.019**
Diabetes	0.022	2.169	0.708	-0.017	2.27	0.778

Figure 1 Study workflow. CVD, cardiovascular disease; DECT, dual-energy computed tomography; WMD, water-calcium material decomposition; VNC, virtual noncontrast; VMI, virtual monochromatic image; DBI, dark-blood imaging; WT, wall thickness; WA, wall area; regress, regression; CNR, contrast-to-noise ratio; CT, computed tomography.

© AME Publishing Company.

Table 1 Basic patient characteristics

Characteristics	Value (n=106)
Age (years)	59±13
Men	56 (52.8)
Body mass index (kg/m^2)	22.42±3.25
Hyperlipidemia	16 (15.1)
Hypertension	28 (26.4)
Diabetes	18 (17.0)
Smoke	26 (24.5)

Data are presented as mean ± standard deviation or n (%).

vessel wall edge, was used by the radiologists: 3= very distinct vessel wall and smooth inner edge, 2= marginally distinct vessel wall and smooth inner edge, 1= unclear vessel wall and coarse inner edge, and 0= completely indistinct vessel wall.

On the identical axial image slice and DFOV used for CNR measurements in WMD and subtraction-based DBI, the WT was manually measured in four directions perpendicular to the center of vessel lumen at 12, 3, 6, and 9 o'clock. The average of the four WT values was recorded as the WT of the descending aorta. The cross-sectional descending WA was calculated according to the following formula:

$$WA = \pi \times \left(WT + \frac{Lumen\ diameter}{2} \right)^2 - \pi \times \left(\frac{Lumen\ diameter}{2} \right)^2 \quad [3]$$

Given the interobserver variability, two radiologists (observers 1 and 2) independently measured the descending aorta WT and lumen diameter.

Collection of CVD risk factor data

CVD risk factor data, including age, gender, smoking status, hypertension, dyslipidemia, and diabetes were collected from the picture archiving and communication system (PACS). Patients with a systolic blood pressure of ≥140 mmHg and/or a diastolic blood pressure of ≥90 mmHg were diagnosed with hypertension. Dyslipidemia was defined as a total cholesterol level of ≥5.2 mmol/L, a triglyceride level of ≥1.7 mmol/L, a low-density lipoprotein cholesterol level of ≥3.4 mmol/L, or a high-density lipoprotein cholesterol level of <1.0 mmol/L as measured by fasting venous serum test indices. Diabetes was defined as a fasting glycated hemoglobin A1C (HbA1c) level of ≥6.5%.

Statistical analysis

All statistical analyses were performed using SPSS 22 (IBM Corp., Armonk, NY, USA). The quantitative image parameters CNR, WT, and WA are presented as the mean and standard deviation and were compared using the analysis of variance (ANOVA) test (for CNR) or *t*-test (for WT and WA). For qualitative data, the subjective scores of WMD and subtraction-based DBI were compared using the Mann-Whitney test. The interobserver agreement for WT was assessed via intraclass correlation coefficients (ICCs). Moreover, the association of WT and WA with CVD risk factors was analyzed by univariate and multiple regression analyses. Linear regression was employed to analyze the correlation between age and the descending aortic WT and WA. The Cohen kappa test was performed to evaluate the interobserver agreement according to the following scheme: poor, κ≤0.40; moderate, κ=0.41–0.60; good, κ=0.61–0.80; and excellent, k=0.81–1.00. P<0.05 was considered statistically significant.

Results

Patients

Of the 106 patients enrolled in our study, there were 56 men and 50 women, with an average age of 59±13 years. The mean body mass index (BMI) was 22.42±3.25 kg/m^2. The high-risk individuals for CVD included 16 cases of hyperlipidemia, 28 cases of hypertension, 18 cases of diabetes, and 26 cases of smoking. The baseline characteristics of the patients are summarized in *Table 1*.

Image quality evaluation of vessel wall imaging

As indicated in *Table 2* and *Figure 2*, the values of $CNR_{wall\text{-}lumen}$ of the descending aorta were 0.59±0.47, 4.36±2.14, and 4.81±3.28 on VNC, subtraction-based DBI, and WMD images, respectively (P<0.001); meanwhile, the corresponding values for $CNR_{wall\text{-}fat}$ were 4.86±1.86, 3.10±1.77, and 3.72±2.45, respectively (P<0.001). For the qualitative evaluation, the image quality scores for observers 1 and 2 were 0.91±0.68 and 1.17±0.73, 2.59±0.49 and 2.47±0.50, and 2.99±0.10 and 2.86±0.35 on VNC, subtraction-based DBI, and WMD images, respectively. *Figure 3* shows the stacked bar graph depicting qualitative scores from the two observers across various vessel wall visualizations. The interobserver agreement for WMD images was good (κ=0.627), and it was moderate for each

© AME Publishing Company.

Table 2 Quantitative and qualitative comparisons of CNR, WT, and WA in subtraction-based DBI, WMD, and VNC

Characteristics	Subtraction-based DBI	WMD	VNC	P	Reference
CNR (wall-fat)	3.41±1.90	4.20±2.67	4.65±1.76	<0.001	
CNR (wall-lumen)	4.19±1.49	4.62±3.61	0.65±0.5	<0.001	
WT (observer 1, mm)	2.18±0.27	2.17±0.27		0.731	2.11±0.06 (F)*; 2.32±0.06 (M)*
WT (observer 2, mm)	2.14±0.27	2.15±0.26		0.867	2.35±0.5**
WA (observer 1, cm^2)	1.55±0.04	1.54±0.03		0.572	1.3±0.3#
WA (observer 2, cm^2)	1.70±0.05	1.71±0.04		0.984	1.5±0.4$
Score (observer 1)	2.59±0.49	2.99±0.10	0.91±0.68		
Score (observer 2)	2.47±0.50	2.86±0.35	1.17±0.73		

Data are presented as mean ± standard deviation. *, represents the average thoracic aorta WT in 196 CVD-free patients on fast spin-echo double-inversion recovery MRI in Li *et al*. (16); **, represents the mean thoracic descending aorta WT using MRI in Malayeri *et al*. (3). # and $ represent the WA in the no-CVD group and the incident CVD group on MRI, respectively, in Neisius *et al.* (10). CNR, contrast-to-noise ratio; WT, wall thickness; WA, wall area; DBI, dark-blood imaging; WMD, water-calcium material decomposition; VNC, virtual noncontrast; F, females; M, males; CVD, cardiovascular disease; MRI, magnetic resonance imaging.

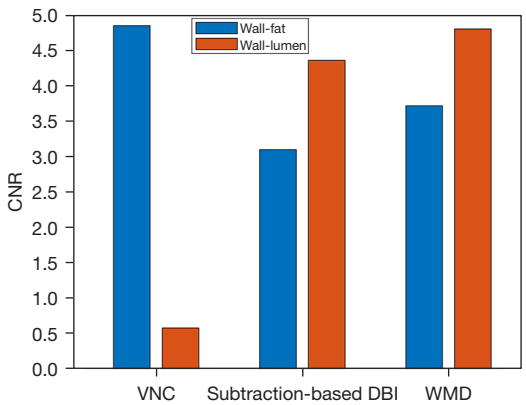

Figure 2 CNRs between the vessel wall and lumen or fat on VNC, subtraction-based DBI and WMD. CNR, contrast-to-noise-ratio; VNC, virtual noncontrast; DBI, dark-blood imaging; WMD, water-calcium material decomposition.

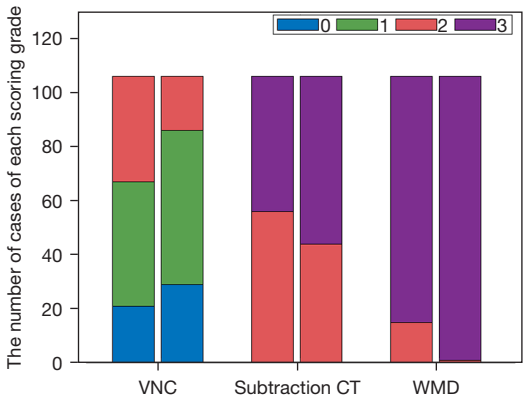

Figure 3 Stacked bar graph of the qualitative scores for different vessel wall imaging modes (left: observer 1; right: observer 2). VNC, virtual noncontrast; CT, computed tomography; WMD, water-calcium material decomposition.

of subtraction-based DBI (κ=0.477) and VNC images (κ=0.56). *Figure 4* shows the representative images of VNC, subtraction-based DBI, and WMD images.

Association of WT and WA with different CVD risk factors

In general, the mean WT values were 2.18±0.27 and 2.17±0.27 mm for observer 1 and 2.14±0.27 and 2.15±0.26 mm for observer 2 on subtraction-based DBI and WMD images, respectively. For the interobserver agreement, the ICCs for WT and WA were 0.70 and 0.90 on subtraction-based DBI and WMD, respectively. *Figure 5A,5B* shows the results of the Bland-Altman analysis for WT. In terms of WA, the measurements were 1.54±0.03 and 1.55±0.04 cm^2 for observer 1 and 1.71±0.04 and 1.70±0.05 cm^2 for observer 2 on WMD images and subtraction-based DBI, respectively. However, the interobserver ICC was 0.99 for both WMD and subtraction-based DBI. *Figure 5C,5D* shows the Bland-Altman of WA differences for WMD and subtraction-based DBI.

Table 3 presents the WT and WA values of patients with different clinical scenarios in median (interquartile range). For WT, patients diagnosed with diabetes had a

© AME Publishing Company.

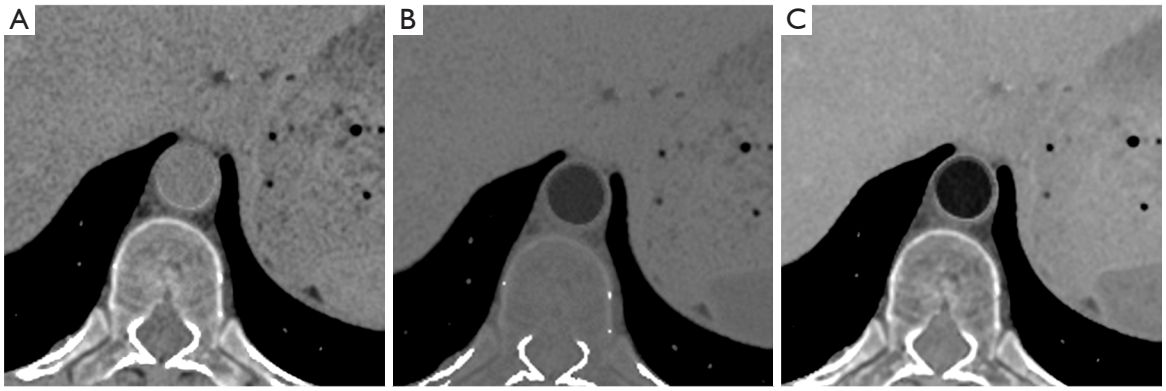

Figure 4 Typical images of VNC, subtraction-based DBI, and WMD. (A) VNC. (B) Subtraction-based DBI. (C) WMD. VNC, virtual noncontrast; DBI, subtraction-based dark-blood imaging; WMD, water-calcium material decomposition.

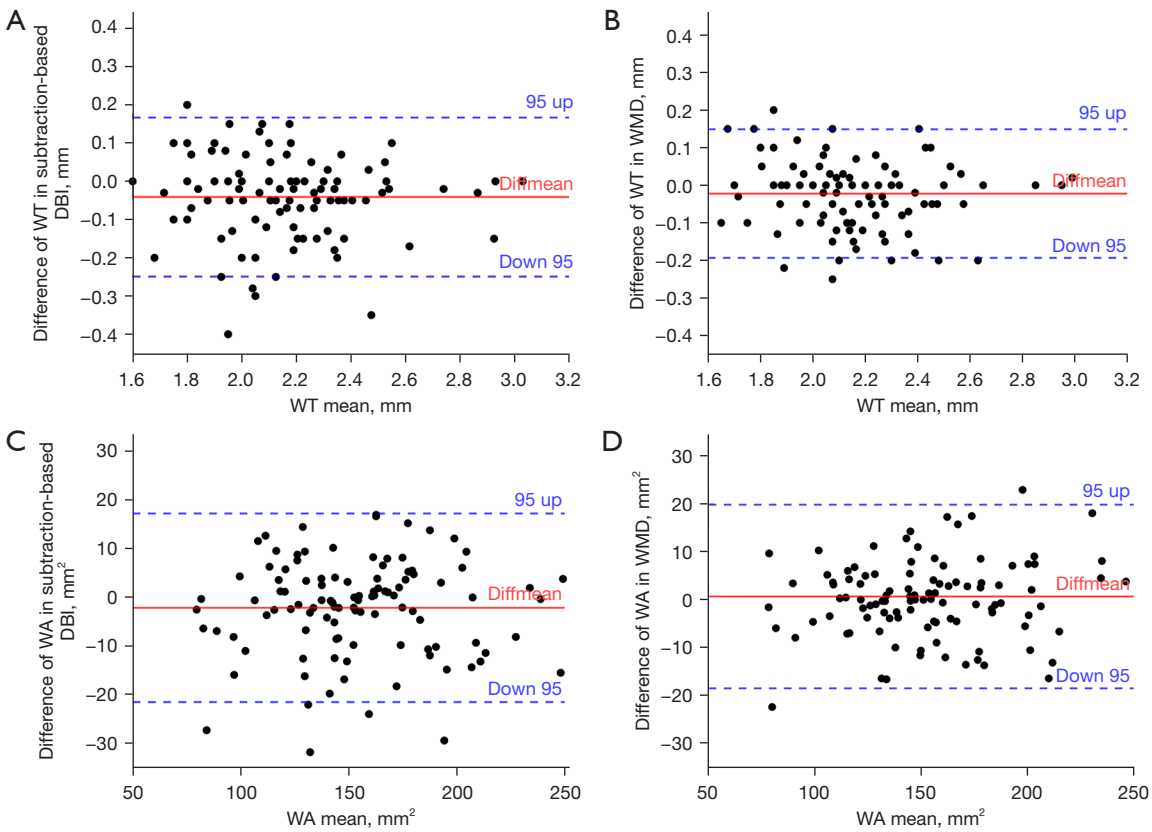

Figure 5 Results of Bland-Altman analyses. (A) WT in subtraction-based DBI. (B) WT in WMD. (C) WA in subtraction-based DBI. (D) WA in WMD. WT, wall thickness; DBI, dark-blood imaging; WMD, water-calcium material decomposition; WA, wall area.

thicker vessel WT of 2.25 (2.08, 2.50) mm as compared to nondiabetic patients [2.13 (1.96, 2.28) mm; P=0.047] in WMD images. Additionally, smokers demonstrated a thicker vessel WT of 2.27 (2.10, 2.47) mm in subtraction-based DBI and of 2.28 (2.10, 2.46) mm in WMD images as compared to nonsmoking patients [subtraction-based DBI: 2.12 (1.95, 2.25) mm, P=0.005; WMD images: 2.09 (1.94, 2.25) mm, P=0.001]. In terms of other CVD risk

© AME Publishing Company.

Table 3 WT and WA comparison between different patient characteristics

Characteristics	Subtraction-based DBI		WMD	
	Values	P	Values	P
WT (mm)				
With hypertension	2.17 (2.04, 2.32)	0.39	2.15 (2.02, 2.36)	0.33
Without hypertension	2.15 (1.96, 2.28)		2.14 (1.98, 2.28)	
With diabetes	2.23 (2.07, 2.46)	0.082	2.25 (2.08, 2.50)	0.047
Without diabetes	2.14 (1.96, 2.28)		2.13 (1.96, 2.28)	
With hyperlipidemia	2.06 (1.94, 2.20)	0.18	2.03 (1.94, 2.18)	0.11
Without hyperlipidemia	2.17 (2.00, 2.31)		2.15 (2.00, 2.30)	
Smoking	2.27 (2.10, 2.47)	0.005	2.28 (2.10, 2.46)	0.001
Nonsmoking	2.12 (1.95, 2.25)		2.09 (1.94, 2.25)	
Male	2.20 (2.00, 2.34)	0.126	2.22 (2.00, 2.35)	0.08
Female	2.13 (1.95, 2.22)		2.10 (1.95, 2.20)	
WA (mm^2)				
With hypertension	173.14 (143.59, 197.19)	0.002	169.34 (143.98, 200.85)	0.002
Without hypertension	144.59 (124.75, 167.37)		145.02 (122.03, 166.53)	
With diabetes	152.17 (141.73, 198.95)	0.21	154.73 (135.14, 192.94)	0.17
Without diabetes	152.40 (128.40, 175.28)		147.12 (122.40, 177.44)	
With hyperlipidemia	142.37 (127.62, 162.04)	0.2	139.59 (124.9, 162.04)	0.12
Without hyperlipidemia	153.49 (129.75, 177.43)		154.15 (128.65, 177.93)	
Smoking	178.88 (162.60, 205.09)	<0.001	181.56 (162.73, 199.99)	<0.001
Nonsmoking	143.44 (126.26, 163.13)		144.37 (121.87, 159.78)	
Male	168.03 (143.12, 194.10)	<0.001	162.14 (144.37, 198.31)	<0.001
Female	140.61 (117.68, 161.37)		136.50 (116.28, 155.76)	

Data are presented as median (interquartile range). WT, wall thickness; WA, wall area; DBI, dark-blood imaging; WMD, water-calcium material decomposition.

factors, there was no significant difference in the univariate analysis. For WA, patients with hypertension [subtraction-based DBI: 173.14 (143.59, 197.19) mm^2; WMD images: 169.34 (143.98, 200.85) mm^2] had a larger WA as compared to nonhypertensive patients [subtraction-based DBI: 144.59 (124.75, 167.37) mm^2, P=0.002; WMD images: 145.02 (122.03, 166.53) mm^2, P=0.002]. Furthermore, the WA of smoking patients, whether in subtraction-based DBI [178.88 (162.60, 205.09) mm^2] or WMD images [181.56 (162.73, 199.99) mm^2], were significantly greater than those of nonsmoking patients [subtraction-based DBI: 143.44 (126.26, 163.13) mm^2, P<0.001; WMD images: 144.37 (121.87, 159.78) mm^2, P<0.001]. In addition, men without CVD [subtraction-based DBI: 168.03 (143.12, 194.10) mm^2; WMD images: 162.14 (144.37, 198.31) mm^2] had a larger WA than did women [subtraction-based DBI: 140.61 (117.68, 161.37) mm^2, P<0.001; WMD images: 136.50 (116.28, 155.76) mm^2, P<0.001]. As shown in *Figure 6A*, the regression analysis between age and average vascular WT was calculated as follows: WT = 0.013 × age + 1.388; this yielded an R^2 of 0.46 for WDM. Meanwhile, for the subtraction-based DBI, the equation was as follows: WT = 0.012 × age + 1.43; this yielded an R^2 of 0.41. In the regression analysis between age and WA (*Figure 6B*), the linear regression functions (WMD: WA = 1.914 × age + 39.20; subtraction-based DBI: WA = 1.875 × age + 42.97)

© AME Publishing Company.

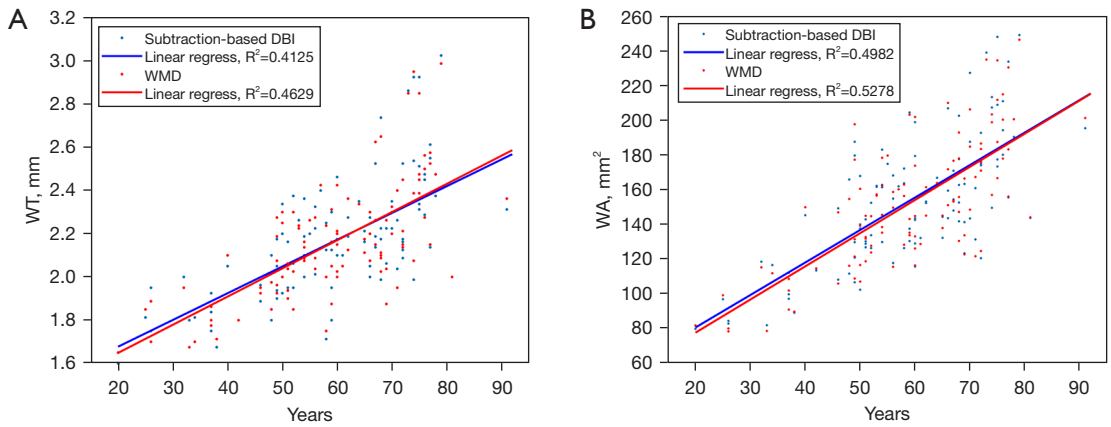

Figure 6 Results of linear regression. (A) Linear regressions between age and WT in subtraction-based DBI and WMD. (B) Linear regression between WA in subtraction-based DBI and WMD. DBI, dark-blood imaging; WMD, water-calcium material decomposition; regress, regression; WT, wall thickness; WA, wall area.

Table 4 Multiple regression analysis of WT and WA with CVD risk factors in both WDM and subtraction-based DBI

Predictor	WMD				Subtraction-based DBI			
	Standardized coefficient	Standard error	P	R^2	Standardized coefficient	Standard error	P	R^2
WT				0.487				0.448
Age (years)	0.641	0.001	<0.001		0.596	0.001	<0.001	
Male	−0.098	0.044	0.252		−0.085	0.046	0.335	
Smoking	0.285	0.051	0.001		0.268	0.053	0.003	
Hypertension	0.046	0.001	0.52		0.114	0.001	0.129	
Diabetes	−0.08	0.019	0.264		−0.145	0.02	0.053	
WA				0.644				0.616
Age (years)	0.615	0.165	<0.001		0.591	0.173	<0.001	
Male	0.165	5.076	0.022		0.155	5.311	0.037	
Smoking	0.262	5.82	<0.001		0.265	6.089	<0.001	
Hypertension	0.105	0.117	0.081		0.148	0.122	0.019	
Diabetes	0.022	2.169	0.708		−0.017	2.27	0.778	

WT, wall thickness; WA, wall area; CVD, cardiovascular disease; WMD, water-calcium material decomposition; DBI, dark-blood imaging.

yielded R^2 values for WMB and subtraction-based DBI of 0.53 and 0.50, respectively. All equations demonstrated that both vessel WT and WA values were positively correlated with age.

The multiple regression analysis is presented in *Table 4*, and the standardized coefficients show that WT values were positively related with age (WMD: 0.641; subtraction-based DBI: 0.595; all P values <0.001) and smoking (WMD: 0.285, P=0.001; subtraction-based DBI: 0.268, P=0.003]. The R^2 values for the models in WMD and subtraction-based DBI were 0.487 and 0.448, respectively. A larger WA in WMD images was also associated with age (standardized coefficient: 0.615; P<0.001), male gender (standardized coefficient: 0.165; P=0.022), and smoking (standardized coefficient: 0.262; P<0.001), with the R^2 value in this model being 0.644. In addition to these factors, higher blood

© AME Publishing Company.

pressure (standardized coefficient: 0.148; P=0.019) was also associated with a larger arterial WA on subtraction-based DBI (R^2=0.616).

Discussion

To the best of our knowledge, this study is the first to demonstrate the feasibility of vessel wall visualization and measurement based on DECT-derived images, including WMD and GE HealthCare's subtraction-based DBI. Notably, discussion in this area has primarily revolved around MRI-derived WT or WA. In addition, we investigated the association between DECT-derived WT/WA and CVD risk factors and examined the potential of WT and WA as image markers for identifying individuals at high risk of CVD.

In terms of the feasibility of vessel wall imaging with either WMD or subtraction-based DBI, both quantitative and qualitative evaluations were performed to assess vessel wall visualization. In this study, the values of $CNR_{wall\text{-}lumen}$ for VNC were significantly lower than those for WMD and subtraction-based DBI. Meanwhile, the WMD images had the highest $CNR_{wall\text{-}lumen}$ values among these three imaging types. Meanwhile, for $CNR_{wall\text{-}fat}$, the VNC had substantially higher values as compared to WMD and subtraction-based DBI, with the values of $CNR_{wall\text{-}fat}$ of subtraction-based DBI being lower than those in WMD images. A previous study reported similar results for both $CNR_{wall\text{-}lumen}$ and $CNR_{wall\text{-}fat}$ in Philip's DBI (14). The qualitative analysis in our study further corroborated these quantitative findings, revealing that WMD provided the best visualization, followed by subtraction-based DBI and VNC. In addition, the enhanced vessel wall visualization in WMD can be attributed to the similarity of spectral curves between calcium and substances present within the vessel. Thus, the water (and calcium) based image appears as if the intravascular material has been virtually removed.

The WT values were 2.17±0.27 and 2.15±0.26 mm for WMD and were 2.18±0.27 and 2.14±0.27 mm for subtraction-based DBI for observers 1 and 2, respectively. Li *et al.* assessed the thoracic aorta WT in 196 CVD-free patients using fast spin-echo double-inversion recovery MRI, reporting an average WT for the descending aorta of 2.11±0.06 mm for females and 2.32±0.06 mm for males (16). Similarly, Malayeri *et al.* reported the mean WT of 2.35±0.5 mm in the thoracic descending aorta of 1,053 CVD-free participants using MRI (3). These results aligned well with our findings. Conversely, another study reported a WT of approximately 1.6 mm, including results from some MR (19,20) and the other dark-blood CT images (14). Variability in imaging and WT measurement methods likely contribute to these discrepancies. The WA values in our study were 1.54±0.03 and 1.71±0.04 cm^2 in WMD and 1.71±0.04/1.70±0.05 cm^2 in subtraction-based DBI for observers 1 and 2, respectively, which were slightly higher than the values of 1.3±0.3 cm^2 in the no-CVD group and 1.5±0.4 cm^2 in the incident CVD group reported by Neisius *et al.* (10). Increasing the sample size in our study may help reduce these discrepancies. It is worth noting that the experienced observer 1 demonstrated WA results closer to those reported by Neisius *et al.* (10).

In the analysis of the correlation of WT and WA with the CVD risk factors, age and smoking emerged as the primary factors contributing to increased WT or WA in this study. Multiple regression analysis revealed that both age and smoking were positively associated with the mean WT and WA values (P<0.05) in both WMD and subtraction-based DBI. The relationship between age and WT is consistent with findings from previous studies, which have reported age to be a significant predictor of thicker WT and an earlier stage of CVD (3,21,22). The variation in WT with age might be explained by the increase in medial thickness, collagenous materials, and calcium deposition, as demonstrated in pathological studies (23,24). Regarding the association between WT and smoking status, prior studies have reported significantly higher WT values in smokers than in nonsmokers (3,18). In our study, smoking was also identified as a predictor of thicker WT or larger WA.

We additionally found that WA was larger in males than in females in both WMD and subtraction-based DBI. WA accounts for both WT and inner diameter, potentially offering greater robustness against measurement variability. The observed relationship between gender and WA in our study aligns with the previous findings indicating a greater WT among men (3,19). In line with this, there is a higher incidence of coronary death rates reported among men across all age groups, as well as a significant correlation between atherosclerosis and acute cardiovascular events (25). However, no statistically significant differences were observed in WT between males and females in either the univariate analysis or multiple regression analysis, which is inconsistent with the findings of other studies. A larger sample size may elucidate any correlations masked by measurement uncertainties.

Furthermore, patients with hypertension had larger WA

© AME Publishing Company.

than did those without hypertension in both WMD and subtraction-based CT images, while hypertension was the predictor of WA only in subtraction-based DBI. As with the gender comparisons, no statistically significant differences in WT were observed between the different blood pressure conditions in either univariate and multiple regression analyses. Previous studies with extensive sample sizes have indicated hypertension to be a predictor of WT (3,26,27), aligning with the observations related to WA in subtraction-based DBI in this study. Hypertension is considered to be a major CVD risk factor that can contribute to vascular remodeling and impaired vascular function (28). Previous research suggests that increased blood pressure elevates vascular wall tension, thereby exacerbating vascular remodeling (29).

Our study involved several limitations which should be addressed. First, only 106 patients were enrolled, whereas previous investigations on the correlation between WT and CVD factors typically involved hundreds to thousands of participants, particularly in multiethnic studies. Our study represents an initial exploration of WT and WA measurement based on DECT-derived WMD or subtraction-based DBI. The correlation of WT and WA with CVD risk factors was investigated to demonstrate the feasibility of using these two DECT-based vessel wall imaging features. Moreover, the limited sample size might have contributed to discrepancies between some of our findings and those in the literature. Therefore, a larger sample size is necessary in future research. Another limitation is the omission of BMI in the correlation analysis. Notably, only three participants had a BMI ≥28 kg/m^2 in this study. Therefore, the BMI factor was not included in the analysis. Finally, due to practical limitations, we lacked reference values for the WT and WA in this patient cohort, such as those obtained from MR vessel wall imaging. To mitigate this limitation, we compared the WT and WA in our study with those of previous research (3,10,16).

Conclusions

We demonstrated the feasibility of DECT-based WMD and subtraction-based DBI for vessel wall imaging using comparisons to VNC. In the patients without CVD, WT, or WA values measured based on these two DECT-derived imaging modes were correlated with age, gender, smoking status, and hypertension. These findings suggest that WT or WA values as measured in DECT-derived WMD and subtraction-based DBI may be valuable for identifying individuals at high risk for CVD within CVD-free populations, a task traditionally completed with MRI.

Acknowledgments

We would like to thank GE HealthCare for providing support in CT scanning technology.
Funding: None.

Footnote

Reporting Checklist: The authors have completed the STROBE reporting checklist. Available at https://qims.amegroups.com/article/view/10.21037/qims-24-1371/rc

Conflicts of Interest: All authors have completed the ICMJE uniform disclosure form (available at https://qims.amegroups.com/article/view/10.21037/qims-24-1371/coif). M.G. and J.L. are currently employees of GE HealthCare, the manufacturer of the CT system used in this study. GE HealthCare had no input regarding the study data or analysis. The other authors have no conflicts of interest to declare.

Ethical Statement: The authors are accountable for all aspects of the work in ensuring that questions related to the accuracy or integrity of any part of the work are appropriately investigated and resolved. This single-center retrospective study was conducted in accordance with the Declaration of Helsinki (as revised in 2013) and was approved by the Ethics Committee of Guangdong Provincial Hospital of Chinese Medicine (No. ZE2023-422-01). The requirement for individual consent was waived due to the retrospective nature of the analysis.

Open Access Statement: This is an Open Access article distributed in accordance with the Creative Commons Attribution-NonCommercial-NoDerivs 4.0 International License (CC BY-NC-ND 4.0), which permits the non-commercial replication and distribution of the article with the strict proviso that no changes or edits are made and the original work is properly cited (including links to both the formal publication through the relevant DOI and the license). See: https://creativecommons.org/licenses/by-nc-nd/4.0/.

References

1. Mensah GA, Fuster V, Roth GA. A Heart-Healthy and

Stroke-Free World: Using Data to Inform Global Action. J Am Coll Cardiol 2023;82:2343-9.
2. Baldassarre D, Amato M, Pustina L, Castelnuovo S, Sanvito S, Gerosa L, Veglia F, Keidar S, Tremoli E, Sirtori CR. Measurement of carotid artery intima-media thickness in dyslipidemic patients increases the power of traditional risk factors to predict cardiovascular events. Atherosclerosis 2007;191:403-8.
3. Malayeri AA, Natori S, Bahrami H, Bertoni AG, Kronmal R, Lima JA, Bluemke DA. Relation of aortic wall thickness and distensibility to cardiovascular risk factors (from the Multi-Ethnic Study of Atherosclerosis [MESA]). Am J Cardiol 2008;102:491-6.
4. Ghaderian M, Barekatain B, Sabri MR, Hovsepian S, Ahmadi A, Dehghan B, Mahdavi C, Ramezani Nezhad D, Arezoo M. Assessment of Vascular Indices by Abdominal Aortic Ultrasonography in Preterm Neonates with Bronchopulmonary Dysplasia. Pediatr Cardiol 2024;45:1816-22.
5. Iwamoto Y, Kimura T, Katakura Y, Tatsumi F, Shimoda M, Nakanishi S, Mune T, Kaku K, Kaneto H. Morphological Differences in the Abdominal Aorta Between Subjects With and Without Type 2 Diabetes. Cureus 2024;16:e68567.
6. Ammirati E, Moroni F, Pedrotti P, Scotti I, Magnoni M, Bozzolo EP, Rimoldi OE, Camici PG. Non-invasive imaging of vascular inflammation. Front Immunol 2014;5:399.
7. Miyagawa M, Kojima K, Takahashi K, Nakajima Y, Migita S, Mizobuchi S, Tanaka Y, Fukumoto K, Arai R, Morikawa T, Mineki T, Murata N, Sudo M, Fukamachi D, Okumura Y. Association Between Aortic Wall Parameters on Multidetector Computed Tomography and Ruptured Plaques By Nonobstructive General Angioscopy. J Am Heart Assoc 2024;13:e033233.
8. Song JW, Pavlou A, Burke MP, Shou H, Atsina KB, Xiao J, Loevner LA, Mankoff D, Fan Z, Kasner SE. Imaging endpoints of intracranial atherosclerosis using vessel wall MR imaging: a systematic review. Neuroradiology 2021;63:847-56.
9. Song JW, Wasserman BA. Vessel wall MR imaging of intracranial atherosclerosis. Cardiovasc Diagn Ther 2020;10:982-93.
10. Neisius U, Gona PN, Oyama-Manabe N, Chuang ML, O'Donnell CJ, Manning WJ, Tsao CW. Relation of MRI Aortic Wall Area and Plaque to Incident Cardiovascular Events: The Framingham Heart Study. Radiology 2022;304:542-50.
11. Rogers IS, Massaro JM, Truong QA, Mahabadi AA, Kriegel MF, Fox CS, Thanassoulis G, Isselbacher EM, Hoffmann U, O'Donnell CJ. Distribution, determinants, and normal reference values of thoracic and abdominal aortic diameters by computed tomography (from the Framingham Heart Study). Am J Cardiol 2013;111:1510-6.
12. Lu Y, Cao R, Jiao S, Li L, Liu C, Hu H, Ma Z, Jiang Y, Chen J. A novel method of carotid artery wall imaging: black-blood CT. Eur Radiol 2024;34:2407-15.
13. Su T, Zhang Z, Chen Y, Wang Y, Li Y, Xu M, Wang J, Li J, Tian X, Jin Z. Dark-Blood Computed Tomography Angiography Combined With Deep Learning Reconstruction for Cervical Artery Wall Imaging in Takayasu Arteritis. Korean J Radiol 2024;25:384-94.
14. Rotzinger DC, Si-Mohamed SA, Shapira N, Douek PC, Meuli RA, Boussel L. "Dark-blood" dual-energy computed tomography angiography for thoracic aortic wall imaging. Eur Radiol 2020;30:425-31.
15. Si K, Wu H, Yang M, Guo Y, Zhang X, Ding C, Xue J, Han P, Li X. Utility of Dark-Blood Dual-Energy CT Images for Predicting Vascular Involvement and R0 Resection in Patients With Pancreatic Cancer. AJR Am J Roentgenol 2023;220:838-48.
16. Li AE, Kamel I, Rando F, Anderson M, Kumbasar B, Lima JA, Bluemke DA. Using MRI to assess aortic wall thickness in the multiethnic study of atherosclerosis: distribution by race, sex, and age. AJR Am J Roentgenol 2004;182:593-7.
17. Qazi S, Massaro JM, Chuang ML, D'Agostino RB Sr, Hoffmann U, O'Donnell CJ. Increased Aortic Diameters on Multidetector Computed Tomographic Scan Are Independent Predictors of Incident Adverse Cardiovascular Events: The Framingham Heart Study. Circ Cardiovasc Imaging 2017;10:e006776.
18. Wolak A, Gransar H, Thomson LE, Friedman JD, Hachamovitch R, Gutstein A, Shaw LJ, Polk D, Wong ND, Saouaf R, Hayes SW, Rozanski A, Slomka PJ, Germano G, Berman DS. Aortic size assessment by noncontrast cardiac computed tomography: normal limits by age, gender, and body surface area. JACC Cardiovasc Imaging 2008;1:200-9.
19. Rosero EB, Peshock RM, Khera A, Clagett P, Lo H, Timaran CH. Sex, race, and age distributions of mean aortic wall thickness in a multiethnic population-based sample. J Vasc Surg 2011;53:950-7.
20. Mani V, Muntner P, Gidding SS, Aguiar SH, El Aidi H, Weinshelbaum KB, Taniguchi H, van der Geest R, Reiber JH, Bansilal S, Farkouh M, Fuster V, Postley JE, Woodward M, Fayad ZA. Cardiovascular

© AME Publishing Company.

magnetic resonance parameters of atherosclerotic plaque burden improve discrimination of prior major adverse cardiovascular events. J Cardiovasc Magn Reson 2009;11:10.
21. Watanabe D, Gando Y, Murakami H, Kawano H, Yamamoto K, Morishita A, Miyatake N, Miyachi M. Longitudinal trajectory of vascular age indices and cardiovascular risk factors: a repeated-measures analysis. Sci Rep 2023;13:5401.
22. Koç AS, Sümbül HE. Age should be considered in cut-off values for increased carotid intima-media thickness. Turk Kardiyol Dern Ars 2019;47:301-11.
23. Marque V, Kieffer P, Atkinson J, Lartaud-Idjouadiene I. Elastic properties and composition of the aortic wall in old spontaneously hypertensive rats. Hypertension 1999;34:415-22.
24. Gaballa MA, Jacob CT, Raya TE, Liu J, Simon B, Goldman S. Large artery remodeling during aging: biaxial passive and active stiffness. Hypertension 1998;32:437-43.
25. Barrett-Connor E. Sex differences in coronary heart disease. Why are women so superior? The 1995 Ancel Keys Lecture. Circulation 1997;95:252-64.
26. Mensel B, Quadrat A, Schneider T, Kühn JP, Dörr M, Völzke H, Lieb W, Hegenscheid K, Lorbeer R. MRI-based determination of reference values of thoracic aortic wall thickness in a general population. Eur Radiol 2014;24:2038-44.
27. Gupta S, Berry JD, Ayers CR, Peshock RM, Khera A, de Lemos JA, Patel PC, Markham DW, Drazner MH. Left ventricular hypertrophy, aortic wall thickness, and lifetime predicted risk of cardiovascular disease:the Dallas Heart Study. JACC Cardiovasc Imaging 2010;3:605-13.
28. Streese L, Pichler FA, Hauser C, Hanssen H. Microvascular wall-to-lumen ratio in patients with arterial hypertension: A randomized controlled exercise trial. Microvasc Res 2023;148:104526.
29. Wan Y, Liu Z, Wu A, Khan AH, Zhu Y, Ding S, Li X, Zhao Y, Dai X, Zhou J, Liu J, Li Y, Gong X, Liu M, Tian XL. Hyperglycemia Promotes Endothelial Cell Senescence through AQR/PLAU Signaling Axis. Int J Mol Sci 2022;23:2879.

Cite this article as: Qi Y, Huang Y, Liu H, Yang Y, Jiang Y, Chen Z, Li L, Guo M, Li J, Zhou D, Liu Y. Association between descending aorta wall thickness or wall area and cardiovascular disease risk factors in cardiovascular disease-free patients: a study based on water-calcium ma-terial decomposition and subtraction-based computed tomography dark-blood imaging. Quant Imaging Med Surg 2025;15(1):370-382. doi: 10.21037/qims-24-1371

© AME Publishing Company.